GEOPHYSICS

Evolving magma temperature and volatile contents over the 2008–2018 summit eruption of Kīlauea Volcano

Josh Crozier*† and Leif Karlstrom

Magma rheology and volatile contents exert primary and highly nonlinear controls on volcanic activity. Subtle changes in these magma properties can modulate eruption style and hazards, making in situ inference of their temporal evolution vital for volcano monitoring. Here, we study thousands of impulsive magma oscillations within the shallow conduit and lava lake of Kīlauea Volcano, Hawai'i, USA, over the 2008–2018 summit eruptive sequence, encoded by "very-long-period" seismic events and ground deformation. Inversion of these data with a petrologically informed model of magma dynamics reveals significant variation in temperature and highly disequilibrium volatile contents over days to years, within a transport network that evolved over the eruption. Our results suggest a framework for inferring subsurface magma dynamics associated with prolonged eruptions in near real time that synthesizes petrologic and geophysical volcano monitoring approaches.

INTRODUCTION

Kīlauea volcano, Hawai'i, USA, is one of the most active, best-monitored, and best-studied volcanoes on Earth (*1*), serving as a focal point for volcanologic research (*2*). However, resolving in situ variation in subsurface magma dynamics remains a challenge at Kīlauea and volcanoes globally (*3*). The 2008–2018 Kīlauea summit eruption represents an opportunity to address this knowledge gap. The eruption involved a persistent lava lake in the Halema'uma'u summit vent and multiple subsurface magma intrusions and East Rift Zone eruptions, ending with a spectacular caldera collapse sequence representing the highest historical sustained eruption rate at Kīlauea (*4*–*6*). Previous studies suggested the main Kīlauea shallow summit magma plumbing system during this time consisted of the 1- to 2-km-deep Halema'uma'u reservoir and the 3- to 5-km-deep South Caldera reservoir (Fig. 1) (*7*, *8*). The Halema'uma'u reservoir and overlying lava lake were continuously connected (*4*) by a ~10-m-wide conduit (*9*). Magma passed through the summit en route to the East Rift Zone, although the nature of hydraulic connections between the summit reservoirs, rift zone, and deeper magma sources is not well known (*8*, *10*).

A wide range of data, interpreted using physical and chemical models, inform this picture of magma dynamics. Transport geometry is constrained primarily through inversion of seismic and geodetic data (*7*, *9*, *11*). Continuous gravity data are only available over limited time segments but constrain the density of magma in the lava lake and suggest temporal variation of up to 1500 kg/m³ (*12*). Analysis of erupted products provides limited temporal and spatial resolution but suggests that Halema'uma'u magma consists of near-liquidus (1150° to 1300°C) crystal-poor basalt outgassed in CO_2 with respect to the primary mantle magma (*13*, *14*). Subsurface magma volatile contents are also indirectly informed by continuous gas emissions (*13*, *15*, *16*). These analyses suggest substantial disequilibrium outgassing or mechanical decoupling of gas bubbles from melt because of continuous

convecting and outgassing (*17*). However, geochemical and geophysical data are rarely combined in a quantitative manner.

Very-long-period (VLP) seismicity, with energy concentrated at periods above 2 s, has the potential to help unify these diverse constraints. VLP seismicity is prevalent at many volcanoes and often inferred to represent transient magma flow (*18*), thus directly probing magma properties and transport geometry in ways not readily obtainable by other geophysical analyses. VLP signals are part of a spectrum of oscillatory motions that can result from impulsive or continuous forcing of magma transport structures (*19*, *20*), but the VLP band is advantageous because it is less sensitive to path distortions from heterogeneous earth structure than shorter period signals.

Multiple resonant modes have been identified at Kīlauea, but the dominant VLP signal is from "conduit-reservoir" resonance, in which stratified magma in the conduit and lake sloshes in and out of the underlying reservoir (Fig. 1) (*9*, *21*, *22*). This resonance occurs sometimes as continuous tremor but most often as discrete minutes-long events triggered both from the lake surface (such as via rockfalls from the crater walls) and from depth (*22*, *23*). Oscillation-restoring forces are from gravity and magma reservoir elasticity, while damping is from viscous drag on the conduit walls. Resonant period is primarily sensitive to conduit length and bulk magma density/density stratification (*9*). Decay rate is quantified by quality factor (the ratio of energy stored per cycle over energy lost per cycle) and is primarily sensitive to conduit radius and apparent magma viscosity. In the shallow Halema'uma'u magma system, where melt composition does not vary much in time or space and where crystal contents are low (*13*, *14*, *24*), magma density is primarily controlled by porosity, and magma viscosity is primarily controlled by porosity and temperature. In chemical equilibrium, gas mass fraction (hence porosity) depends on total volatile mass fraction and pressure-dependent solubility of dominant volatile species (H_2O, CO_2, and sulfur) (*25*).

VLP seismicity at Kīlauea thus reflects evolving magma thermal and chemical state as well as transport structures. Over the 2008–2018 Kīlauea eruption, thousands of conduit-reservoir resonance events provide an unprecedented record of time-evolving subsurface magma transport.

Department of Earth Sciences, University of Oregon, Eugene, OR, USA.
*Corresponding author. Email: jcrozier@usgs.gov
†Present address: U.S. Geological Survey California Volcano Observatory Moffett Field, CA, USA.
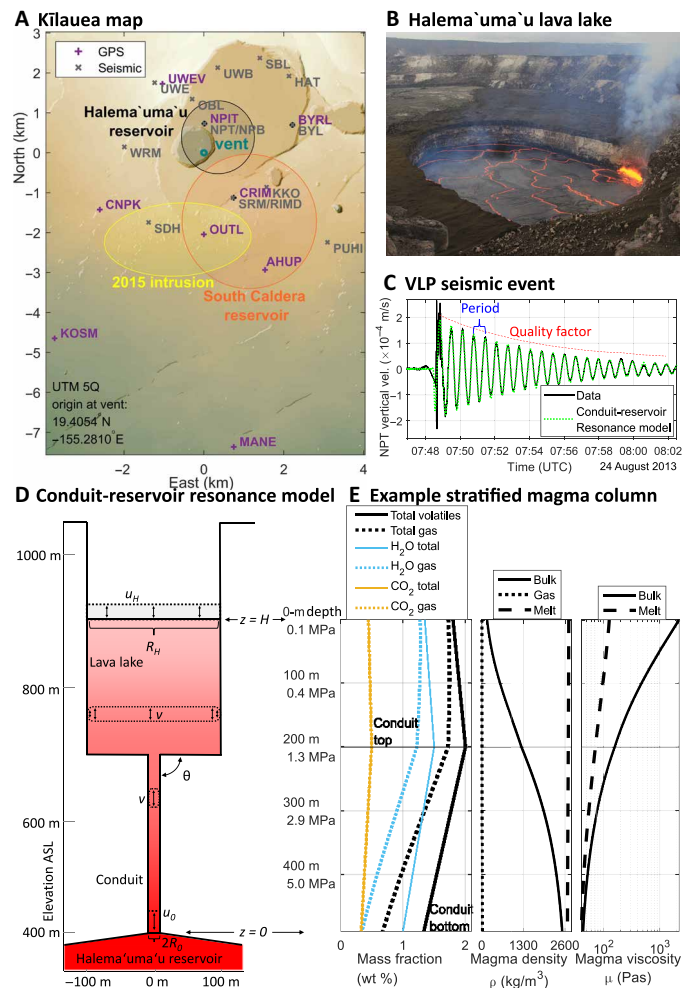
Fig. 1. Kīlauea map and magma dynamics model. (**A**) Map including the Halemaʻumaʻu vent, inferred shallow magma storage zones, GNSS stations, and seismometers used in the VLP catalog (*22*). (**B**) Typical lava lake activity on 13 February 2017 U.S. Geological Survey (USGS). (**C**) Seismic waveform from a VLP conduit-reservoir resonance event along with a model solution for reference fixed parameter inversion results forced with a Gaussian pressure perturbation (fig. S1). UTC, universal time coordinated. (**D**) Conduit-reservoir resonance model with approximate 2018 magma system geometry; black arrows illustrate vertical sloshing of the stratified magma column. ASL, above sea level. (**E**) Magmastatic depth profiles from piecewise linear total (dissolved plus exsolved) volatile mass fractions at a uniform temperature of 1200°C.

Approach: Inferring magma properties from geophysical data

Figure 2 outlines our workflow. We first conduct kinematic elastic inversions between 2008 and 2018 of continuous Global Navigation Satellite System (GNSS) ground deformation data (figs. S3 and S4) (*26*) for shallow magma reservoir pressure histories. In particular, Halemaʻumaʻu reservoir pressure constrains magma column density in the overlying summit lava lake and conduit. Summit deformation at Kīlauea is complex: To resolve Halemaʻumaʻu reservoir pressure, we build on constraints from previous geodetic studies (*7*, *11*, *27*) and include three known deformation sources (*26*).

We next use a perturbation approach to model transient flow associated with conduit-reservoir magma resonance (Fig. 1) (*26*), extending previous analyses (*9*, *21*). We treat fluid properties of the

multiphase magma as functions of magmastatic pressure (an approximation given slow exchange flow within the conduit/lava lake (*28*)), temperature, and vertically stratified total volatile mass fractions (CO_2 + H_2O; Fig. 1 and fig. S2), neglecting crystals and assuming an average melt composition based on 2008–2010 Halemaʻumaʻu samples (*13*, *25*, *29*–*31*). We use this model to invert for magma properties from Halemaʻumaʻu reservoir pressure, lava lake elevation and areal extent (*4*, *32*), and the resonant period and quality factor of VLP seismic events cataloged over 2008–2018 by (*22*) (Fig. 2) (*26*).

Resolving time evolution of shallow magma properties at Kīlauea is a long-standing challenge (*9*, *33*, *34*). We focus on shorter-term changes in multiphase magma properties by assuming a fixed magma system geometry based on previous inversions (*7*, *9*, *11*). Four additional assumptions are made to facilitate unique inversions for magma properties (Supplementary Text) (*26*): (i) Temperature is spatially uniform in the conduit and lake. This is justified because the conduit undergoes quasi-steady exchange flow/mixing (*35*), and the lake contributes negligibly to viscous damping. (ii) Magma in the conduit/lake has a fixed total (dissolved + exsolved) H_2O/CO_2 mass ratio. Volatile composition could vary over time but is unconstrained in our model without additional data, so we fix volatile ratios based on erupted products and gas emissions (*13*, *14*, *36*). (iii) Total volatile mass fraction varies linearly with depth (Fig. 1) subject to stable stratification, which should be approximately valid for the largely quiescent magma column. (iv) Total volatile mass fraction at the lake surface is constant. While there is known to be some variation in porosity near the lake surface from continuous gravity data (*37*), these data are not available over most of the time span. In addition, our model exhibits minimal sensitivity to density stratification within the lake; it is primarily sensitive to average density (which controls the magmastatic pressure load of the lake on the conduit).

We test different fixed parameter combinations and conduct an a posteriori assessment of these assumptions. The magma properties we invert for are (i) magma temperature, (ii) conduit average total volatile mass fraction X^{avg}, and (iii) total volatile mass fraction stratification (difference between conduit top and conduit bottom) ΔX. We note that while the magma temperature parameter is applied to the whole magma column, the model is primarily sensitive to conduit temperature. We also note that because of the trade-offs between volatile contents at the bottom and top of the lava lake, ΔX should be considered to represent a general volatile stratification over the whole magma column (conduit and lava lake).

RESULTS

For our reference fixed parameters, Fig. 3 shows the timeline of GNSS inversion results and VLP magma resonance inversion results, along with other data. Shaded regions in Fig. 3 show the envelope of inversion results obtained by varying individual fixed parameters over feasible ranges, as detailed in the Supplementary Text (fig. S5). Evolution of magma system geometry, which is not considered in our inversions, is more likely to affect trends in inversion results over long (year or more) time scales. In particular, inversion results with the reference fixed parameters are likely not reliable in 2009 to early 2010 and mid-2011 (Discussion). On short time scales, noise in input data likely contributes to scatter and outliers in the inversion results. We thus focus most analysis on temporally averaged values and, in particular, on the relative variability in these values
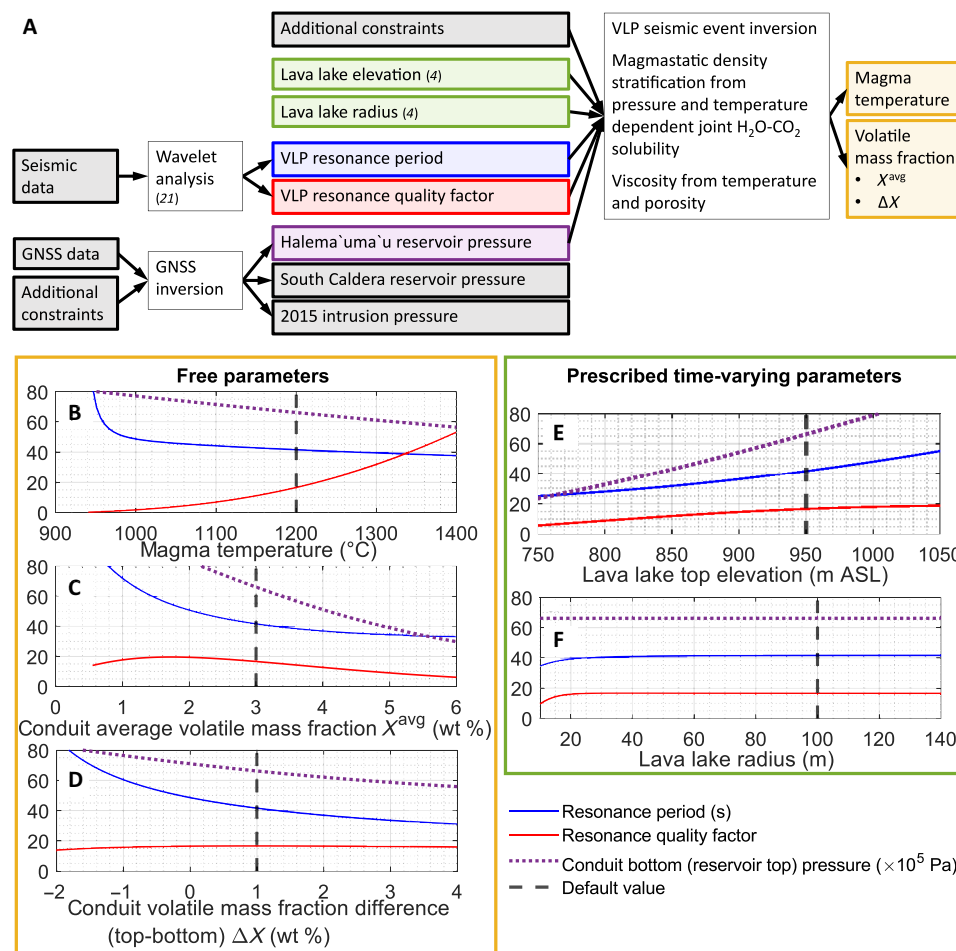
Fig. 2. Inversion approach. (**A**) Simplified flowchart of methods and data input/output. Additional constraints on GNSS inversions are from previous geodetic studies (*11*, *27*, *57*, *60*). Additional constraints on VLP magma resonance inversions are from previous modeling (*9*), gravity data (*37*), and geochemical (gas and ejecta) data (*13*, *16*, *24*, *36*). (**B** to **F**) Conduit-reservoir resonance period and quality factor, plus conduit bottom pressure, as a function of the parameters varied to fit Kīlauea VLP seismic and geodetic data. Variations in lava lake elevation and (assumed uniform) radius are prescribed from measurements (*4*, *32*). Dashed black lines indicate default values used in the other plots.

over time scales of a year or less rather than their absolute value at a given time. Figure 4 shows amplitude spectra, coherence, and phase lags between data sets with 95% significance thresholds (Supplementary Text). Additional analyses are shown in figs. S6 to S8.

As expected for an open-vent magma system, Halema'uma'u reservoir pressure is well correlated with lava lake elevation over time scales from days to about a year (Figs. 3 and 4) (*4*, *22*). Strong coherence between Halema'uma'u and South Caldera reservoir pressures over time scales of days to months (Fig. 4 and fig. S6) suggests that magma is often transferred between the reservoirs, although the anticorrelation implies hydraulic disequilibrium. This could indicate an intermittent connection, consistent with the unsteady connectivity inferred during hours- to days-long "deflation-inflation" events (*6*, *8*, *38*). We are not aware of any other settings where a consistent anticorrelation is observed between different magma reservoirs at the same volcano, although intermittent hydraulic connections have been inferred between Kīlauea and Mauna Loa (*39*), as well as at other volcanoes such as Soufriére Hills (*40*) and Etna (*41*).

Different fixed parameters affect the absolute value of inverted magma temperature, but the pattern of relative temporal variation is robust, and the magnitude of such changes varies by less than ~20°C (Fig. 3 and fig. S5). Inverted temperature is primarily sensitive to conduit radius; decreasing radius by 10 m (to 5 m) uniformly increases temperatures by ~60°C, while increasing radius by 10 m (to 25 m) uniformly decreases temperatures by ~40°C. Conduit magma temperatures span the full 1150° to 1300°C range of Halema'uma'u magma storage temperatures previously estimated from ejecta geothermometry (*13*, *24*), although it is difficult to make a direct comparison given uncertainty in the depths and/or time scales recorded by geothermometers.

On time scales from days to months, temperature exhibits up to 100°C variation (Fig. 3), corresponding to up to an order of magnitude variation in magma viscosity (figs. S2 and S8). Temperature and resonant quality factor are strongly correlated (fig. S6), which suggests that temperature is a primary driver of variations in magma viscosity. The dominance of temperature is unexpected because porosity has previously been proposed as a likely source of variation
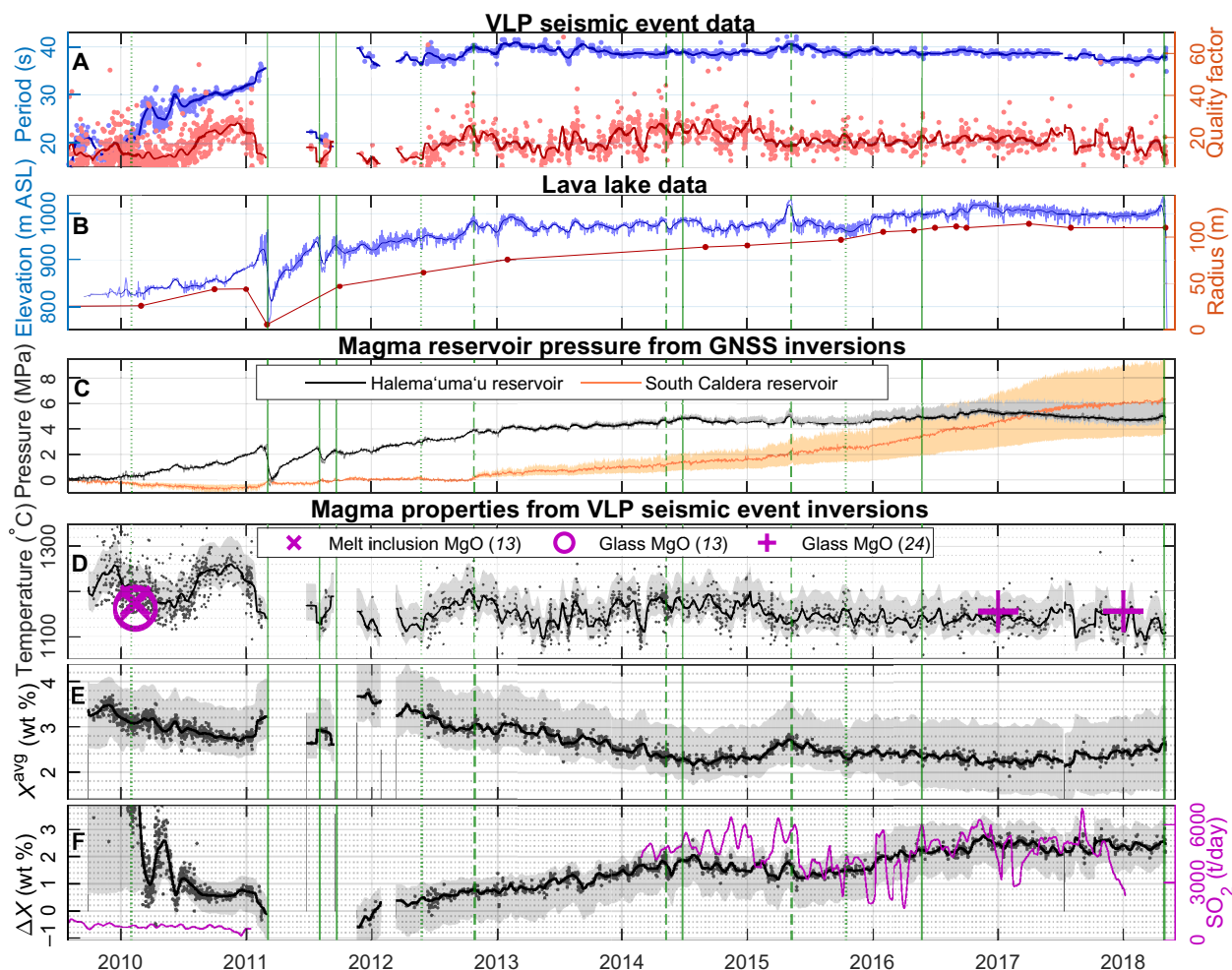
Fig. 3. Time-series data and inversion results. Inverted relative changes in magma properties are from our reference fixed parameters (Fig. 1 and table S1). Dots represent individual VLP seismic events, bold lines are 30-day moving averages, while vertical green lines are East Rift Zone eruptions (solid), summit intrusions (dashed), and slow-slip events (dotted) (*4*). (**A**) VLP seismic event resonance period and quality factor (*22*). (**B**) Lava lake elevation and mean radius (*4, 32*) (**C**) GNSS inverted reservoir pressure changes, set to zero at the 7 March 2011 lava lake draining. Shaded areas indicate possible variation with different South Caldera reservoir geometries tested (Supplementary Text). (**D**) Inverted conduit magma temperature, with MgO thermometry for comparison (*13, 24*). The shaded area indicates possible variation with all fixed model parameter values tested (Supplementary Text). (**E** and **F**) Inverted conduit total volatile contents, with 30-day moving average SO_2 emissions for comparison (*15, 16*) and possible variation shown in shaded areas. Values from 2009 to early 2010 are unreliable because of exact solutions not being obtainable with the fixed parameters chosen.

in VLP quality factor (*21*) and is known to vary significantly as bubbles rise and accumulate (*28, 37*).

Different fixed parameters affect the inverted absolute value of X^{avg} by up to ~1 weight % (wt %), but the pattern of relative temporal variation is robust and the magnitude of such changes varies by less than ~0.4 wt % (Fig. 3 and fig. S5). Similarly, different fixed parameters affect the inverted absolute value of ΔX by up to ~1 wt %, but the pattern of relative temporal variation is robust, and the magnitude of such changes varies by less than ~0.2 wt % (Fig. 3 and fig. S5). Over most of the timeline X^{avg} is greater than the inferred primary magma volatile mass fraction of 1 to 2 wt % , a notable accumulation particularly because some of the primary CO_2 may have already been lost at depth (*14, 36, 42*). In addition, ΔX is mostly similar to or larger than inferred primary magma volatile mass fraction. Together, these indicate substantial departures from equilibrium outgassing, with an accumulation of volatiles in the upper conduit and lava lake.

On time scales of days to months, X^{avg} varies by up to ~0.6 wt %, and ΔX varies by up to ~1 wt % (Fig. 3). That this temporal variation is similar to the inferred primary magma's total volatile mass fraction of 1 to 2 wt % (*36, 42*) suggests strong variations in the outgassing regime (*14*). The only volatile species with continuous emission measurements that can be compared with ΔX and X^{avg} is SO_2. SO_2 has roughly similar solubility to H_2O in mafic melts (*43*) and so will approximately trade-off with H_2O in our model. SO_2 emissions exhibit strong variation (an order of magnitude or more) on time scales from days to years (*15, 16*). We do not observe consistently strong coherence between ΔX or X^{avg} and SO_2 emissions (fig. S6), although several pronounced increases in either ΔX or X^{avg} do correspond to increases in SO_2 (e.g., April 2015, January 2016, October 2016, and August 2017). Inconsistent coherence could partly reflect the high uncertainty in SO_2 emission data, although we note that gas emissions from the lava lake surface will not necessarily directly correlate with the amount of volatiles accumulated in the
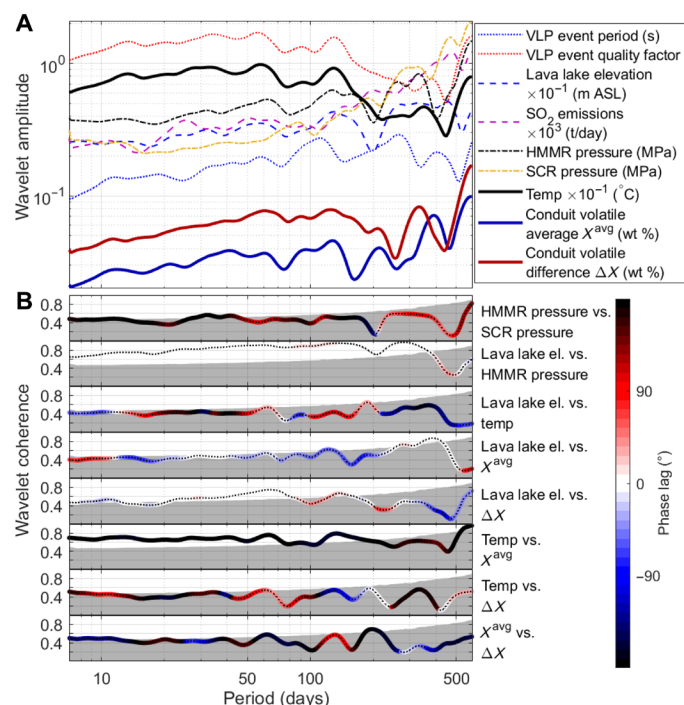
Fig. 4. Wavelet amplitude spectra and coherence. (**A**) Amplitude spectra of resonance properties (*22*), lava lake elevation (*4, 32*), SO$_2$ emissions (*15, 16*), GNSS inverted Halemaʻumaʻu (HMMR) and South Caldera (SCR) reservoir pressures, and VLP magma resonance inverted magma properties. (**B**) Magnitude squared coherence colored by phase lag. The gray area is beneath the 95% significance threshold. Positive phase lags indicate that the second variable trails the first. Data before December 2011 were excluded from this analysis.

magma column. The strong in-phase coherence between Halemaʻumaʻu reservoir pressure (or lava lake elevation) and ΔX on time scales of less than 90 days (Fig. 4) suggests that volatiles build up in the upper conduit/lake as magma accumulates in the Halemaʻumaʻu system rather than maintaining a steady volatile mass balance through the shallow magma column. This could reflect an increase in volatile flux (e.g., from magma recharge), but could also be caused by less efficient outgassing through the lava lake as it fills.

DISCUSSION

Halemaʻumaʻu magma mass balance

Maintaining a persistent lava lake for a decade requires a remarkable thermal and mechanical balance. Relatively constant magma supply from depth is needed to drive continuous convection, but supply must be countered by sufficient outflux to prevent conditions leading to violent eruption. Ground deformation and VLP seismicity provide a quasi-continuous probe of magma properties that facilitates interrogation of the multiscale processes maintaining (and modulating) this balance within the Halemaʻumaʻu reservoir during an extended eruption.

In general, magma reservoir pressure can change even without any magma input due to gas exsolution and (to a lesser extent) crystallization. However, because the low-viscosity mafic melt and open-vent structure of Halemaʻumaʻu facilitates gas escape, reservoir pressurization has been inferred to reflect accumulation of melt due to changes in either influx (e.g., recharge from the South Caldera

reservoir or deeper storage regions) or outflux (e.g., to the East Rift Zone) (*4, 44*). For example, the inferred causes of the May 2015 summit intrusion, the 2018 eruption, and the prevalent hours- to days-long deflation-inflation summit deformation events are months of increased magma influx (*4, 6, 27*), months of reduced magma outflux (*45*), and transient restrictions of magma influx or outflux (*6, 8, 38*). However, the general controls on magma mass balance over days to years are unknown. The 60- and 130-day period spectral peaks in Halemaʻumaʻu reservoir pressure (also apparent in temperature, ΔX, and X^{avg}) (Fig. 4) may indicate dominant time scales for such changes in influx-outflux (*4*). Quasi-periodic deformation and/or eruptive activity on similar time scales has also been observed at other volcanoes (*46, 47*).

We might expect magma recharge to increase conduit temperature, although this would depend on the temperature and influx of recharging magma and also its path through the ~4 km^3 of near-liquidus magma in the Halemaʻumaʻu reservoir (*11, 24*). The inferred 2011–2012 average magma supply rate of ~10^9 kg/day (*34*) would permit complete exchange with the ~10^{10} kg of magma in the conduit and lava lake over a week. However, if this injected magma were uniformly mixed with the magma in the reservoir (~10^{13} kg assuming a density of 2500 kg/m^3) at a 100°C temperature difference, the mixture temperature would only increase by ~0.01°C/day (neglecting latent heat and outflow). Given the poor coherence between Halemaʻumaʻu reservoir pressure (or lava lake elevation) and temperature (Fig. 4), we expect that melt injected into the Halemaʻumaʻu reservoir generally either was not appreciably hotter than existing magma and/or was not directly routed to the conduit.

One prominent exception that could exemplify an influx of hotter melt from depth is the persistent ~100°C increase in temperature 6 months before the March 2011 Kamoamoa fissure eruption. There was no corresponding increase in volatile mass fractions, potentially due to deeper separation and upward flux of volatiles over the preceding months of elevated volatile mass fractions. Temperature then dropped by ~100°C in the months leading up to the eruption, which we expect relates to lava lake downwelling rather than magma influx/outflux, as discussed in the next section. Another potential example of hot melt influx is the ~90°C increase in temperature between the May 2012 slow-slip event on Kīlauea's south flank décollement and the October 2012 intrusion, although there was also no corresponding increase in volatile mass fractions. The temperature increase supports previous suggestions that slow-slip events are linked to magmatism (*48*), although we do not see similar temperature increases immediately following the 2010 or 2015 slow-slip events.

It is less obvious what changes in magma properties might be expected from decreased magma outflux, so we use the 2018 eruption as a case study. The months of pressurization preceding the eruption are accompanied by a decrease in magma temperature and increase in X^{avg}, but these do not clearly stand out from the background variation over the preceding year (Fig. 3). The lack of clear changes in magma properties is consistent with the idea that the 2018 eruption was triggered by decreasing outflux rather than by recharge (*45*) and, by extension, suggests that outflux does not necessarily drive notable changes in shallow magma properties. The May 2014 and May 2015 intrusions were also preceded by a month of Halemaʻumaʻu reservoir pressurization without other clearly associated changes in the summit magma system. The lack of clear changes in magma properties would seem to suggest they were

induced by decreased magma outflux, although at least in 2015, changes in East Rift Zone lava effusion were not apparent (*4*, *6*, *27*). The June 2014 and May 2016 PuʻuʻŌʻō vent openings were not preceded by notable pressurization of the shallow summit magma system, suggesting they were not primarily caused by increased melt flux from the summit but rather by processes along the rift zone.

Shallow magma dynamics

Our results illuminate shallow fluid dynamic processes underlying a persistent lava lake. Observed covariation of parameters in our inversions suggests that volatile mass fraction and temperature in the conduit and lava lake vary in ways not always directly related to Halemaʻumaʻu reservoir magma influx/outflux. We infer that such variation occurs because of unsteady exchange flow between the conduit and Halemaʻumaʻu reservoir (*49*), as well as because of changing convective efficiency in the lava lake and/or surface crust dynamics (which influence the outgassing rate and efficiency of heat loss to the atmosphere and host rock) (*4*, *50*).

The negative correlation on time scales of months or less between X^{avg} and temperature (Fig. 4 and fig. S6) likely reflects such dynamics, because relatively poor coherence with Halemaʻumaʻu reservoir pressure (or lava lake elevation) indicates neither X^{avg} nor temperature is primarily driven by magma mass balance. Simple thermal arguments suggest likely causes of temperature variation. Atmospheric heat exchange at the lake surface will be dominated by radiative heat flux $\phi_r = A\epsilon\sigma(T_{surf}^4 - T_{atm}^4)$, where ϕ_r is ~1 gigawatt (GW) for lake surface area $A \approx 10^4$ m², thermal emissivity $\epsilon \approx 0.8$, Stefan-Boltzmann constant $\sigma = 5.7\times10^{-8}$ W m⁻² K⁻⁴, and average surface temperature $T_s \approx 700$°C (*50*). Heat flux to the host rock depends on hydrothermal circulation, but can be approximated with an effective thermal conductivity $\phi_c = k_e\Delta T/\Delta L$, where ϕ_c is 10 to 1000 W/m² for k_e of 2 to 20 W m⁻¹ C⁻¹ (*51*) and temperature gradient $\Delta T/\Delta L$ of 10 to 100°C/m (*52*). Total heat transfer rate Φ from the conduit and lake (surface area ~10^5 m²) and from the Halemaʻumaʻu reservoir (surface area ~10^7 m²) is 1 to 100 megawatt (MW) and 0.1 to 10 GW, respectively. Neglecting latent heat, average temperature of a magma mass M will decrease as $dT/dt = \Phi/(c_pM)$. For specific heat $c_p \approx 1000$ J kg⁻¹ K⁻¹, average temperature of the ~10^{10} kg of magma in the conduit and lake could decrease by ~10°C/day, whereas average temperature of the ~10^{13} kg of magma in the Halemaʻumaʻu reservoir would only decrease by ~0.01 to 1°C/month. We thus expect the prevalent temperature drops of 100°C or more that occur over days to weeks represent downwelling of magma that cooled in the upper lava lake. Episodic downwelling suggests episodically decoupled convection cells in the lava lake rather than a convective regime that settles persistently into one of the configurations previously proposed (*6*, *53*). This mechanism likely explains the ~100°C temperature drop preceding the March 2011 Kamoamoa fissure eruption, where a changing convective regime is perhaps related to the rapidly filling lava lake and/or high short-term (hours to days) variability in lava lake elevation during this time. In some other cases, rapid lava lake draining might also induce downwelling of cool magma. This downwelling could explain the days-long temperature decreases accompanying the October 2012 and May 2014 intrusions, although if so, it is interesting that the 2015 intrusion did not cause a temperature drop.

An evolving magma plumbing system geometry

Given a consistent open hydraulic connection between the Halemaʻumaʻu reservoir and lava lake, the weakening coherence between them over years or longer (Fig. 4) could represent changes either in the magma column density or in the relation between reservoir pressure and ground deformation (a function of geometry and poroviscoelastic rock properties). Our fixed geometry inversions test the former and show that for a range of feasible fixed parameter values (fig. S5), very high values of X^{avg} and/or ΔX are required over some portion of the timeline (e.g., 2009 through mid-2010 for reference parameters). These volatile contents would correspond to a foam in the upper conduit and lava lake with an average porosity in excess of 90%. Available constraints from gravity data (*12*) suggest average porosity in the lava lake of only up to 70%, so the higher values inferred at early times are likely unrealistic. We thus expect subsurface magma plumbing system geometry evolved over time, which could also contribute to the weak coherence between inverted South Caldera and Halemaʻumaʻu reservoir pressures over long time scales (fig. 4).

Changes in conduit length (reservoir-roof depth) of ~10 m or changes in conduit radius of ~1 m could measurably affect VLP resonance period and quality factor at Kīlauea (fig. S5). Such changes might occur gradually because of processes such as viscous deformation of the host rock, thermal/mechanical erosion, or crystallization. Geometry could also change abruptly because of host rock failure or opening/closing of hydraulically connected dikes/sills. To fit the low VLP periods in 2009–2010 with realistic volatile contents, a ~100-m-higher reservoir roof elevation (510 instead of 410 m above sea level, which is within estimated uncertainty (*11*)) and/or strongly tapered conduit (e.g., top radius <5 m and bottom radius >15 m) is required (fig. S9). It is unlikely that the roof of an ellipsoidal reservoir would have grown downward this much over year time scales because of crystallization, so it may have been shallower throughout the eruption. In this case, the drastic change in VLP periods over the early part of the eruption likely represents an evolving conduit geometry due to some combination of a widening upper conduit and a change in conduit length due to a changing dip angle and reservoir attachment depth. A shallow dike/sill above the main Halemaʻumaʻu reservoir could have also impacted the resonance (*54*); this would potentially be consistent with some seismic inversions (*21*, *33*), but such additional source complexity is not needed according to other seismic and geodetic inversions (*7*, *9*, *11*).

Toward a new generation of volcano monitoring

Resolving the dynamics of subsurface magma transport is a grand challenge that dictates hazard forecasting efficacy as well as connections between active volcanic processes and the geologic record. Inferring relative changes in magma properties over days to months by identifying the fluid origin of VLP seismic events represents a concrete step toward unifying the inversion of geophysical and geochemical data. In particular, we have resolved temperature changes of over 100°C that likely reflect both convective overturns and magma recharge. We have also resolved stratified volatile profiles that represent a highly disequilibrium outgassing regime. Volatile contents vary by over 1 wt % on time scales from days to months, revealing an unsteady shallow volatile mass balance. We have also inferred an evolving magma system geometry, highlighting the need to develop models and data sets that can deconvolve changing fluid properties from changing transport pathways.

Incorporating additional data would yield even more precise constraints on multiphase magma properties and their depth variation. For example, continuous gravity data would provide independent constraints on magma density in the lake. Video of lake surface

oscillations could independently constrain vertical motions of the lake and triggering mechanisms of VLP events. In addition, surface gas emission data could constrain volatile stratification and outgassing/convective regimes if combined with models for gas flux through the magma column.

Similar VLP events have been detected at Vanuatu and Erebus volcanoes (55, 56) and are expected at open-vent volcanoes generally (20), suggesting that this type of analysis could be adapted to improve near real-time monitoring at other eruptions. These data will inform basic volcano science and lead to better understanding of physical controls on volcanic eruptions.

MATERIALS AND METHODS
GNSS inversions
To obtain time series of pressure change in the Halemaʻumaʻu reservoir, we must consider other known sources of ground deformation at the Kīlauea summit: the South Caldera reservoir (7, 8), 2015 intrusion (27), and steady slip along the south flank décollement (fig. S3) (57). We assume a temporally fixed geometry for the three magma reservoirs (Fig. 1 and Supplementary Text) but constrain the 2015 intrusion to be an active deformation source only over May 13 to 17 (27). We adopt the 2-km-deep 4-km^3 ellipsoidal Halemaʻumaʻu reservoir geometry and 3-GPa rock shear modulus from (11), consistent with other studies (7, 9, 10, 58, 59). We assume a horizontal centroid location of the South Caldera reservoir based on inversions of (60); depth and geometry are less well constrained, so we choose a reference 20-km^3 sphere centered 4 km deep and test different values based on published ranges (7, 10, 58). We fixed the 2015 intrusion geometry following (27).

Reservoir pressures are found using linear least square inversions (Supplementary Text) of daily average surface position solutions from the Nevada Geodetic Laboratory (61) for GNSS stations within a few kilometers of the reservoirs (Fig. 1), corrected for steady background south flank slip with the multicomponent dislocation model of (57) (figs. S3 and S4). We use an approximate solution for deformation associated with a pressurized ellipsoid in an elastic half space (62) for each of the three magma bodies.

Conduit-reservoir magma oscillation model
We model VLP seismic events as small amplitude, isothermal, and incompressible oscillatory magma flow within a lava lake–conduit–reservoir system. The model is extended from (20) to include inertial effects in the lava lake and experimentally constrained models for multiphase magma properties (Supplementary Text). We consider an inclined radially symmetric magma column encompassing the lava lake and conduit, underlain by a reservoir within elastic rocks (Fig. 1).

The magma column prior to VLP events is assumed magmastatic, justified because fluid particle velocities associated with resonance are larger than background exchange flow (20). During VLPs, viscous drag is determined from shear stress at the magma column wall where a no-slip velocity condition is enforced. With z and r distance parallel and perpendicular to the magma column axis (a function of conduit dip from horizontal θ), linearized conservation of momentum (primed variables) around a background state (bars) is

$$\frac{d\langle v'\rangle}{dt}\overline{\rho} \;=\; \langle u'\rangle \sin(\theta)\frac{d\overline{\rho}}{dz}g - \sin(\theta)\frac{\partial p'}{\partial z} + \frac{2\mu}{R}\frac{\partial v'}{\partial r}\bigg]_R \qquad (1)$$

Here, $\langle u'\rangle$ is the cross-sectionally averaged conduit-parallel fluid particle displacement (so the orientation of $\langle u'\rangle$ is a function of θ), v' is the conduit-parallel fluid particle velocity, $\langle v'\rangle$ is the cross-sectionally averaged v' (the time derivative of $\langle u'\rangle$), ρ is the magma density, p' is the pressure perturbation, μ is the dynamic viscosity, and R is the conduit radius. Conservation of mass is $\langle u'\rangle = \langle u_0'\rangle R_0^2/R^2$, where subscript 0 indicates evaluation at the bottom of the magma column (Fig. 1).

We assume equilibrium joint solubility of CO_2 and H_2O in Halemaʻumaʻu composition melts (13) as a function of pressure and gas composition (25) (Supplementary Text and fig. S2). We neglect other volatile species as they have generally lower concentrations and/or poorly constrained solubility at Kīlauea (13, 43). We assume ideal gas behavior and consider melt density a function of pressure, temperature, and composition (29). Melt viscosity $\mu_l(z)$ is assumed to be a function of temperature and dissolved H_2O (31). The impact of bubbles on apparent magma viscosity depends on the magnitude of capillary forces (30). For expected strain rates of $\sim 10^{-1}$ s^{-1} associated with slow exchange flow in the conduit, bubbles less than ~ 10 cm across will increase apparent viscosity approximately according to $\mu = \mu_l/(1 - \overline{\phi})$(fig. S2), where $\overline{\phi}(z)$ is the background magma porosity (30).

For conduit-reservoir resonance, pressure at the base of the magma column is $P_0' = -\pi R_0^2\langle u_0'\rangle\sin(\theta_0)/C_r$ (20), where C_r is the total storativity of the reservoir (reservoir volume change per unit pressure increase). The Halemaʻumaʻu reservoir assumed here corresponds to a "buoyancy-dominated" limit where reservoir pressure changes have a negligible effect on the magma column during VLPs (Supplementary Text) (9). Pressure at the top of the magma column is $P_H' = P_{ex} + \langle u_H'\rangle\sin(\theta_H)\overline{\rho}_H g$, where subscript H indicates evaluation at the top of the magma column, and $P_{ex}(t)$ is the external forcing (Fig. 1). This system is equivalent to a driven harmonic oscillator with frequency-dependent damping and exhibits exponentially decaying oscillations in response to an impulsive forcing (fig. S1). We find the resonant period and quality factor by solving numerically for the free response of the system (Supplementary Text).

VLP seismic event inversions
We assume a temporally fixed magma plumbing system geometry, except for lava lake radius and surface elevation, which are interpolated from measurements (Supplementary Text) (4, 32). We choose reference fixed parameters based on previous constraints where available. Where minimal constraints are available, we test a range of values and select combinations that produce feasible inversion results over most of the timeline, as detailed in the Supplementary Text. We approximate the lava lake and conduit as cylinders, with a reference conduit radius of 15 m and conduit dip of 90° from horizontal (Fig. 1 and table S1).

We conduct inversions using the conduit-reservoir resonance model for the three free parameters (temperature, X^{avg}, and ΔX) from the three target values for each VLP seismic event: conduit bottom (Halemaʻumaʻu reservoir top) pressure, resonance period, and resonance quality factor (Fig. 2). We use an iterative nonlinear trust-region-reflective solver to find the combination of free parameter values that minimizes misfit E

$$E = \frac{|\omega - \omega^*|}{\omega^*} + \frac{|Q - Q^*|}{Q^*} + \frac{|\overline{P}_0 - \overline{P}_0^*|}{\overline{P}_0^*} \qquad (2)$$

where vertical bars indicate absolute value, asterisks indicate observed/target values, Q is the resonance quality factor, ω is the resonance angular frequency, and $\bar{P}_0$ is the magmastatic pressure at the bottom of the conduit (top of the reservoir). To prevent unfeasible solutions, we impose bounds on the search space such that volatile mass fraction at all depths is between 0 and 7 wt % and temperature is between 900° and 1600°C. In most cases, there is an exact solution ($E = 0$), although for some VLP events (e.g., in 2009 and early 2010), exact solutions do not exist for the reference parameters, and the solver will find a local minimum instead. Grid searches indicate that the misfit spaces are convex, so the solver is finding unique global minima and/or unique exact solutions. Time-series analysis methods used to interpret inversions are detailed in the Supplementary Text.

SUPPLEMENTARY MATERIALS
Supplementary material for this article is available at https://science.org/doi/10.1126/sciadv.abm4310

REFERENCES AND NOTES

1. M. Garcia, A. Pietruszka, M. Norman, M. Rhodes, Kīlauea's Puʻu ʻŌʻō Eruption (1983–2018): A synthesis of magmatic processes during a prolonged basaltic event. *Chem. Geol.* **581**, 120391 (2021).
2. J. Pallister, S. R. McNutt, in *The Encyclopedia of Volcanoes* (Elsevier, 2015), pp. 1151–1171.
3. M. Manga, S. A. Carn, K. V. Cashman, A. B. Clarke, C. B. Connor, K. M. Cooper, T. Fischer, B. Houghton, J. B. Johnson, T. A. Plank, D. C. Roman, P. Segall, *Volcanic Eruptions and Their Repose, Unrest, Precursors, and Timing* (National Academies, 2017).
4. M. Patrick, D. Swanson, T. Orr, A review of controls on lava lake level: Insights from Halemaʻumaʻu Crater, Kīlauea Volcano. *Bull. Volcanol.* **81**, 13 (2019).
5. C. Neal, C. A. Neal, S. R. Brantley, L. Antolik, J. L. Babb, M. Burgess, K. Calles, M. Cappos, J. C. Chang, S. Conway, L. Desmither, P. Dotray, T. Elias, P. Fukunaga, S. Fuke, I. A. Johanson, K. Kamibayashi, J. Kauahikaua, R. L. Lee, S. Pekalib, A. Miklius, W. Million, C. J. Moniz, P. A. Nadeau, P. Okubo, C. Parcheta, M. R. Patrick, B. Shiro, D. A. Swanson, W. Tollett, F. Trusdell, E. F. Younger, M. H. Zoeller, E. K. Montgomery-Brown, K. R. Anderson, M. P. Poland, J. L. Ball, J. Bard, M. Coombs, H. R. Dietterich, C. Kern, W. A. Thelen, P. F. Cervelli, T. Orr, B. F. Houghton, C. Gansecki, R. Hazlett, P. Lundgren, A. K. Diefenbach, A. H. Lerner, G. Waite, P. Kelly, L. Clor, C. Werner, K. Mulliken, G. Fisher, D. Damby, The 2018 rift eruption and summit collapse of Kīlauea Volcano. *Science* **363**, 367–374 (2019).
6. M. P. Poland, A. Miklius, I. A. Johanson, K. R. Anderson, A decade of geodetic change at Kīlauea's summit—Observations, interpretations, and unanswered questions from studies of the 2008–2018 Halemaʻumaʻu eruption. *U.S. Geol. Surv. Prof. Pap.* pp1867G (2021).
7. M. P. Poland, A. Miklius, E. K. Montgomery-Brown, Characteristics of Hawaiian volcanoes. *U.S. Geol. Surv. Prof. Pap.* **1801**, 179–234 (2014).
8. A. Anderson, J. Foster, N. Frazer, Implications of deflation-inflation event models on Kīlauea Volcano, Hawaiʻi. *J. Volcanol. Geotherm. Res.* **397**, 106832 (2020).
9. C. Liang, J. Crozier, L. Karlstrom, E. Dunham, Magma oscillations in a conduit-reservoir system, application to very long period (VLP) seismicity at basaltic volcanoes: 2. Data inversion and interpretation at Kīlauea Volcano. *J. Geophys. Res. Solid Earth* **125**, e2019JB017456 (2020).
10. T. Wang, Y. Zheng, F. Pulvirenti, P. Segall, Post-2018 caldera collapse re-inflation uniquely constrains Kīlauea's magmatic system. *J. Geophys. Res. Solid Earth* **126**, e2021JB021803 (2021).
11. K. R. Anderson, I. A. Johanson, M. R. Patrick, M. G. Segall, M. P. Poland, E. K. Montgomery-brown, A. Miklius, Magma reservoir failure and the onset of caldera collapse at Kīlauea Volcano in 2018. *Science* **366**, eaaz1822 (2019).
12. M. Poland, D. Carbone, Insights into shallow magmatic processes at Kīlauea Volcano, Hawaiʻi, from a multiyear continuous gravity time series. *J. Geophys. Res. Solid Earth* **121**, 5477–5492 (2016).
13. M. Edmonds, I.R. Sides, D.A. Swanson, C. Werner, R.S. Martin, T.A. Mather, R.A. Herd, R.L. Jones, M.I. Mead, G. Sawyer, T.J. Roberts, A.J. Sutton, T. Elias, Magma storage, transport and degassing during the 2008–10 summit eruption at Kīlauea Volcano, Hawaiʻi. *Geochim. Cosmochim. Acta* **123**, 284–301 (2013).
14. A. H. Lerner, P. J. Wallace, T. Shea, A. J. Mourey, P. J. Kelly, P. A. Nadeau, T. Elias, C. Kern, L. E. Clor, C. Gansecki, R. L. Lee, L. R. Moore, C. A. Werner, The petrologic and degassing behavior of sulfur and other magmatic volatiles from the 2018 eruption of Kīlauea, Hawaiʻi: Melt concentrations, magma storage depths, and magma recycling. *Bull. Volcanol.* **83**, 43 (2021).
15. T. Elias, A. J. Sutton, Sulfur Dioxide emission rates from Kīlauea Volcano, Hawaiʻi, 2007–2010. *U.S. Geol. Surv. Open-File Rep.* **2012-1107**, 25 (2012).
16. T. Elias, C. Kern, K. Horton, A. Sutton, H. Garbeil, Measuring SO2 emission rates at Kīlauea Volcano, Hawaii, using an array of upward-looking UV spectrometers, 2014–2017. *Front. Earth Sci.* **6**, 214 (2018).
17. S. Vergniolle, C. Jaupart, Dynamics of degassing at Kilauea Volcano, Hawaii. *J. Geophys. Res.* **95**, 2793 (1990).
18. B. Chouet, R. Matoza, A multi-decadal view of seismic methods for detecting precursors of magma movement and eruption. *J. Volcanol. Geotherm. Res.* **252**, 108–175 (2013).
19. L. Karlstrom, E. M. Dunham, Excitation and resonance of acoustic-gravity waves in a column of stratified, bubbly magma. *J. Fluid Mech.* **797**, 431–470 (2016).
20. C. Liang, L. Karlstrom, E. Dunham, Magma oscillations in a conduit-reservoir system, application to very long period (VLP) seismicity at basaltic volcanoes: 1. Theory. *J. Geophys. Res. Solid Earth* **125**, e2019JB017437 (2020).
21. B. Chouet, P. Dawson, Very long period conduit oscillations induced by rockfalls at Kilauea Volcano, Hawaii. *J. Geophys. Res. Solid Earth* **118**, 5352–5371 (2013).
22. J. Crozier, L. Karlstrom, Wavelet-based characterization of very-long-period seismicity reveals temporal evolution of shallow magma system over the 2008–2018 eruption of Kilauea Volcano. *J. Geophys. Res. Solid Earth* **126**, e2020JB020837 (2021).
23. P. Dawson, B. Chouet, Characterization of very-long-period seismicity accompanying summit activity at Kīlauea Volcano, Hawaiʻi: 2007–2013. *J. Volcanol. Geotherm. Res.* **278-279**, 59–85 (2014).
24. C. Gansecki, R. L. Lee, T. Shea, S. P. Lundblad, K. Hon, C. Parcheta, The tangled tale of Kīlauea's 2018 eruption as told by geochemical monitoring. *Science* **366**, eaaz0147 (2019).
25. G. Iacono-Marziano, Y. Morizet, E. Le Trong, F. Gaillard, New experimental data and semi-empirical parameterization of H2O–CO2 solubility in mafic melts. *Geochim. Cosmochim. Acta* **97**, 1–23 (2012).
26. Materials and methods are available as supplementary materials at the science website.
27. M. J. Bemelmans, E. de Zeeuw-van Dalfsen, M. P. Poland, I. A. Johanson, Insight into the May 2015 summit inflation event at Kīlauea Volcano, Hawaiʻi. *J. Volcanol. Geotherm. Res.* **415**, 107250 (2021).
28. A. C. Fowler, M. Robinson, Counter-current convection in a volcanic conduit. *J. Volcanol. Geotherm. Res.* **356**, 141–162 (2018).
29. R. A. Lange, I. S. E. Carmichael, Densities of Na2O-K2O-CaO-MgO-FeO-Fe2O3-Al2O3-TiO2-SiO2 liquids: New measurements and derived partial molar properties. *Geochim. Cosmochim. Acta* **51**, 2931–2946 (1987).
30. E. W. Llewellin, M. Manga, Bubble suspension rheology and implications for conduit flow. *J. Volcanol. Geotherm. Res.* **143**, 205–217 (2005).
31. D. Giordano, J. K. Russell, D. B. Dingwell, Viscosity of magmatic liquids: A model. *Earth Planet. Sci. Lett.* **271**, 123–134 (2008).
32. M. Patrick, D. Swanson, T. Orr, F. Younger, W. Tollett, Elevation of the lava lake in Halemaʻumaʻu crater, Kilauea Volcano, from 2009 to 2018. *U.S. Geol. Surv.* (2022).
33. B. Chouet, P. Dawson, M. James, S. Lane, Seismic source mechanism of degassing bursts at Kilauea Volcano, Hawaii: Results from waveform inversion in the 10–50 s band. *J. Geophys. Res.* **115**, B09311 (2010).
34. K. Anderson, M. Poland, Bayesian estimation of magma supply, storage, and eruption rates using a multiphysical volcano model: Kīlauea Volcano, 2000–2012. *Earth Planet. Sci. Lett.* **447**, 161–171 (2016).
35. M. DiBenedetto, Z. Qin, J. Suckale, Crystal aggregates record the pre-eruptive flow field in the volcanic conduit at Kīlauea, Hawaii. *Sci. Adv.* **6**, eabd4850 (2020).
36. M. Edmonds, I. Sides, J. Maclennan, in *Hawaiian Volcanoes* (American Geophysical Union, 2015), chap. 15, pp. 323–349.
37. M. Poland, D. Carbone, Continuous gravity and tilt reveal anomalous pressure and density changes associated with gas pistoning within the summit lava lake of Kīlauea Volcano, Hawaiʻi. *Geophys. Res. Lett.* **45**, 2319–2327 (2018).
38. K. Anderson, M. Poland, J. Johnson, A. Miklius, in *Hawaiian Volcanoes* (American Geophysical Union, 2015), chap. 11, pp. 229–250.
39. M. Shirzaei, T. R. Walter, R. Bürgmann, Coupling of Hawaiian volcanoes only during overpressure condition. *Geophys. Res. Lett.* **40**, 1994–1999 (2013).
40. D. Elsworth, G. Mattioli, J. Taron, B. Voight, R. Herd, Implications of magma transfer between multiple reservoirs on eruption cycling. *Science* **322**, 246–248 (2008).
41. M. Aloisi, M. Mattia, C. Ferlito, M. Palano, V. Bruno, F. Cannavò, Imaging the multi-level magma reservoir at Mt. Etna volcano (Italy). *Geophys. Res. Lett.* **38**, L16306 (2011).
42. K. Anderson, M. Poland, Abundant carbon in the mantle beneath Hawaiʻi. *Nat. Geosci.* **10**, 704–708 (2017).
43. A. Burgisser, M. Alletti, B. Scaillet, Simulating the behavior of volatiles belonging to the C–O–H–S system in silicate melts under magmatic conditions with the software D-Compress. *Comput. Geosci.* **79**, 1–14 (2015).
44. D. Dzurisin, M. Poland, in *Field Volcanology: A Tribute to the Distinguished Career of Don Swanson* (Geological Society of America, 2019), vol. 538, pp. 275–295.

45. M. R. Patrick, B. F. Houghton, K. R. Anderson, M. P. Poland, E. Montgomery-Brown, I. Johanson, W. Thelen, T. Elias, The cascading origin of the 2018 Kīlauea eruption and implications for future forecasting. *Nat. Commun.* **11**, 5646 (2020).

46. S. Hautmann, J. Gottsmann, R. S. J. Sparks, A. Costa, O. Melnik, B. Voight, Modelling ground deformation caused by oscillating overpressure in a dyke conduit at Soufrière Hills Volcano, Montserrat. *Tectonophysics* **471**, 87–95 (2009).

47. A. Toombs, G. Wadge, Co-eruptive and inter-eruptive surface deformation measured by satellite radar interferometry at Nyamuragira volcano, D.R. Congo, 1996 to 2010. *J. Volcanol. Geotherm. Res.* **245-246**, 98–122 (2012).

48. E. Montgomery-brown, M. Poland, A. Miklius, in *Hawaiian Volcanoes: From Source to Surface* (Blackwell, 2015), vol. 208, pp. 269–288.

49. J. Suckale, Z. Qin, D. Picchi, T. Keller, I. Battiato, Bistability of buoyancy-driven exchange flows in vertical tubes. *J. Fluid Mech.* **850**, 525–550 (2018).

50. J. Thompson, M. Ramsey, Spatiotemporal variability of active lava surface radiative properties using ground-based multispectral thermal infrared data. *J. Volcanol. Geotherm. Res.* **408**, 107077 (2020).

51. H. Schmeling, G. Marquart, A scaling law for approximating porous hydrothermal convection by an equivalent thermal conductivity: Theory and application to the cooling oceanic lithosphere. *Geophys. J. Int.* **197**, 645–664 (2014).

52. P. Hsieh, S. Ingebritsen, Groundwater inflow toward a preheated volcanic conduit: Application to the 2018 eruption at Kīlauea Volcano, Hawai'i. *J. Geophys. Res. Solid Earth* **124**, 1498–1506 (2019).

53. M. Patrick, T. Orr, D. Swanson, E. Lev, Shallow and deep controls on lava lake surface motion at Kīlauea Volcano. *J. Volcanol. Geotherm. Res.* **328**, 247–261 (2016).

54. M. McQuillan, L. Karlstrom, Fluid resonance in elastic-walled englacial transport networks. *J. Glaciol.* **67**, 1–14 (2021).

55. R. Aster, S. Mah, P. Kyle, W. McIntosh, N. Dunbar, J. Johnson, M. Ruiz, S. McNamara, Very long period oscillations of Mount Erebus Volcano. *J. Geophys. Res. Solid Earth* **108**, 1–22 (2003).

56. T. Shreve, R. Grandin, M. Boichu, E. Garaebiti, Y. Moussallam, V. Ballu, F. Delgado, F. Leclerc, M. Vallée, N. Henriot, S. Cevuard, D. Tari, P. Lebellegard, B. Pelletier, From prodigious volcanic degassing to caldera subsidence and quiescence at Ambrym (Vanuatu): The influence of regional tectonics. *Sci. Rep.* **9**, 18868 (2019).

57. S. Owen, P. Segall, M. Lisowski, A. Miklius, R. Denlinger, M. Sako, Rapid deformation of Kilauea Volcano: Global positioning system measurements between 1990 and 1996. *J. Geophys. Res. Solid Earth* **105**, 18983–18998 (2000).

58. S. Baker, F. Amelung, Top-down inflation and deflation at the summit of Kīlauea Volcano, Hawai'i observed with InSAR. *J. Geophys. Res. Solid Earth* **117**, B12406 (2012).

59. A. Roman, P. Lundgren, Dynamics of large effusive eruptions driven by caldera collapse. *Nature* **592**, 392–396 (2021).

60. M. Poland, A. Miklius, A. Jeff Sutton, C. Thornber, A mantle-driven surge in magma supply to Kīlauea Volcano during 2003–2007. *Nat. Geosci.* **5**, 295–300 (2012).

61. G. Blewitt, W. Hammond, C. Kreemer, Harnessing the GPS data explosion for interdisciplinary science. *Eos* **99**, 10.1029/2018EO104623 (2018).

62. M. Battaglia, P. F. Cervelli, J. R. Murray, dMODELS: A MATLAB software package for modeling crustal deformation near active faults and volcanic centers. *J. Volcanol. Geotherm. Res.* **254**, 1–4 (2013).

63. P. Segall, *Earthquake and Volcano Deformation* (Princeton Univ. Press, 2010).

64. J. R. Womersley, Method for the calculation of velocity, rate of flow and viscous drag in arteries when the pressure gradient is known. *J. Physiol.* **127**, 553–563 (1955).

65. Y. Zhang, Z. Xu, M. Zhu, H. Wang, Silicate melt properties and volcanic eruptions. *Rev. Geophys.* **45**, RG4004 (2007).

66. M. T. Mangan, K. V. Cashman, D. A. Swanson, in *U.S. Geological Survey Professional Paper 1801-8* (U.S. Geological Survey), pp. 323–354 (2014).

67. H. Mader, E. Llewellin, S. Mueller, The rheology of two-phase magmas: A review and analysis. *J. Volcanol. Geotherm. Res.* **257**, 135–158 (2013).

68. J. Suckale, B. H. Hager, L. T. Elkins-Tanton, J. C. Nave, It takes three to tango: 2. Bubble dynamics in basaltic volcanoes and ramifications for modeling normal Strombolian activity. *J. Geophys. Res. Solid Earth* **115**, 7410 (2010).

69. J. E. Gardner, R. A. Ketcham, G. Moore, Surface tension of hydrous silicate melts: Constraints on the impact of melt composition. *J. Volcanol. Geotherm. Res.* **267**, 68–74 (2013).

70. C. A. Williams, G. Wadge, An accurate and efficient method for including the effects of topography in three-dimensional elastic models of ground deformation with applications to radar interferometry. *J. Geophys. Res. Solid Earth* **105**, 8103–8120 (2000).

71. A. Grinsted, J. C. Moore, S. Jevrejeva, Application of the cross wavelet transform and wavelet coherence to geophysical time series. *Nonlinear Processes Geophys.* **11**, 561–566 (2004).

ScienceAdvances

Evolving magma temperature and volatile contents over the 2008–2018 summit eruption of Kīlauea Volcano

Josh CrozierLeif Karlstrom

View the article online
https://www.science.org/doi/10.1126/sciadv.abm4310
Permissions
https://www.science.org/help/reprints-and-permissions

Use of this article is subject to the Terms of service